A Silicon Photonic RF Phase Shifter With Linear Phase Response and Low RF Power Variation

Qihang Shang, Yanping Yu, Yong Zhang, Yu He, Shaohua An, Xinhong Jiang, and Yikai Su, *Senior Member, IEEE*

***Abstract*— We propose and experimentally demonstrate a microwave photonic phase shifter based on a tunable silicon photonic interleaver. This device consists of a microring resonator, a tunable interleaver, and a 2 × 1 multimode interferometer (MMI). By thermally tuning the interleaver, a linear phase shift of 188° is realized with a linearity of 0.08 and a radio-frequency (RF) power variation within 1 dB for a 40-GHz signal.**

***Index Terms*— Interleaver, linear phase shift, microwave photonics, silicon.**

I. Introduction

INTEGRATED microwave photonics has been a topic of interest owing to its compact footprint, low transmission loss and electromagnetic interference immunity [1]. Microwave photonics can find many applications, such as phased array beamforming [2] and microwave photonic filters [3]. Recently, phased array beamforming technologies at the millimeter-wave frequency have attracted much attention for the fifth generation (5G) wireless networks [4].

Microwave photonic phase shifters are key components for optical beamforming in phased array antennas [1], [2]. Conventional phase shifters are limited to narrow band operations due to the nonlinear phase responses [4], [5]. In recent years, some schemes have been proposed to realize radio frequency (RF) photonic phase shifters with large linear phase-shifting properties. A dual-microring resonator that can achieve a full 360° quasi-linear phase shift was demonstrated with an RF power variation of lower than 2 dB [6]. Since this structure employs two cascaded microring resonators (MRRs), it is required to align and maintain the resonance wavelengths of the two resonators. A phase shifter with a semi-linear phase shift of 360° was proposed based on silicon graphene waveguides consisting of two ring cavities [7].

To achieve a phase shifter with a linear phase response and a low RF power variation, here we propose an on-chip RF phase shifter based on a tunable silicon photonic interleaver. An interleaver is a periodic optical filter in wavelength, which combines or separates wavelength-division multiplexed (WDM) signals [8]. Interleavers are usually designed to possess flat-top passband transmission. Since ideal bandpass filters are supposed to be dispersionless [9], many interleavers are designed with high-linearity phase responses in the passbands [10]. In our previous work [11], we presented an interleaver that consists of an interfering loop containing a Fabry–Perot cavity formed by two Sagnac loops. The group delay characteristic analyzed in [11] shows that the interleaver has almost linear phase responses in the passbands, which can be used to realize a linear phase shifter. In addition, the flat-top passbands of the interleaver enable a low RF power variation of the phase shifter.

In this letter, we propose and experimentally demonstrate an interleaver-based phase shifter (IBPS). The IBPS is composed of an add-drop MRR, an interleaver, and a 2×1 multimode interferometer (MMI). The two tones of an input RF photonic signal are separated by the add-drop MRR and combined by an MMI. The thermo-optic effect of the interleaver is used to shift one of the tones. A full 360° phase shift for a 40-GHz RF photonic signal can be realized, while a linear phase shift of 188° is achieved with a linearity of 0.08 and a <1-dB RF power variation. The proposed device was fabricated on a silicon-on-insulator (SOI) platform which can be integrated with photonic and electronic circuits.

II. Principle and Simulations

The schematic diagram of the proposed IBPS is shown in Fig. 1. The device includes an add-drop MRR, an interleaver and a 2×1 MMI. The add-drop MRR is used to separate the two tones of the input RF photonic signal. The interleaver contains a directional coupler and two Sagnac loops. Based on the scatter matrix method, the field transmission function of the interleaver is given by [11]:

$$T = \frac{(t_1^2 - k_1^2)(t_2^2 - k_2^2)a_1^2a_2^2a_3 - 4t_1k_1t_2k_2a_1^2a_2(1 + a_2^2a_3^2)}{1 + 4t_2^2k_2^2a_2^2a_3^2}, \tag{1}$$

where t_i and k_i ($t_i^2 + k_i^2 = 1$, $i = 1, 2$) represent the transmission and coupling coefficients of the directional couplers, respectively. $a_i = \exp(-\alpha l_i - j\beta l_i)$ ($i = 1, 2, 3$) are the transmission factors associated with the waveguides. l_i ($i = 1, 2, 3$), α and β are the lengths, the loss factor and the propagation constant of the waveguides, respectively. Fig. 2(a) shows the simulated transmission spectrum of the interleaver.

Manuscript received November 28, 2018; revised March 9, 2019; accepted March 14, 2019. Date of publication March 20, 2019; date of current version April 22, 2019. This work was supported in part by the National Natural Science Foundation of China under Grant 61835008 and Grant 61860206001 and in part by the Science and Technology Commission of Shanghai Municipality under Grant 17500710900 and Grant 16XD1401400. *(Corresponding author: Yikai Su.)*

The authors are with the State Key Laboratory of Advanced Optical Communication Systems and Networks, Department of Electronic Engineering, Shanghai Jiao Tong University, Shanghai 200240, China (e-mail: qihangshang@sjtu.edu.cn; ypyu0811@sjtu.edu.cn; yongzhang@sjtu.edu.cn; yuhe2015@sjtu.edu.cn; shaohuaan@sjtu.edu.cn; jiangxinhong@sjtu.edu.cn; yikaisu@sjtu.edu.cn).

Color versions of one or more of the figures in this letter are available online at http://ieeexplore.ieee.org.

Digital Object Identifier 10.1109/LPT.2019.2906373

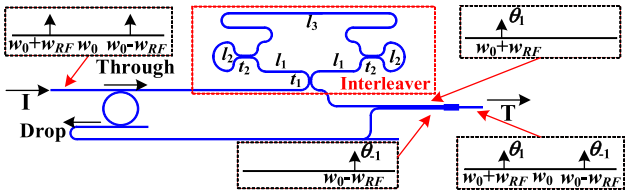

Fig. 1. Schematic diagram of the IBPS.

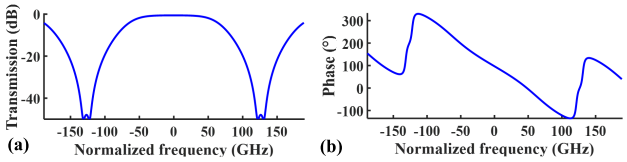

Fig. 2. Simulated (a) transmission spectrum and (b) phase response of the interleaver.

The loss factor α and the group index n_g are assumed to be 2 dB/cm and 4.352, respectively. The free spectral range (FSR $= \lambda^2/(n_g L)$) is determined by the cavity length of the FP cavity ($L = l_2 + l_3$). l_1, l_2 and l_3 are designed to be 41.89 μm, 64.83 μm and 207.55 μm, respectively, leading to a ~2-nm FSR of the interleaver as a choice to keep a low tuning power while maintaining the linearity of the device. A maximally-flat response of the interleaver is realized by setting $t_1 = 0.924$, and $t_2 = 0.977$. Linear phase responses in the passbands are shown in Fig. 2(b). The transmission-coefficient deviations may affect the performance of the IBPS. When t_1/t_2 increases, the power variation firstly increases and then decreases in a certain spectral range around the central wavelength of the interleaver. The increasing of t_2 leads to a better linearity in the passband.

To demonstrate a photonic RF phase shifter, optical carrier suppression (OCS) modulation is employed to generate two optical tones. A 40-GHz frequency interval is used in the following discussion. The input optical field of the IBPS can be expressed as:

$$E_{in}(t) = A_{-1}\exp[j(\omega_0 - \omega_{RF})t] + A_1\exp[j(\omega_0 + \omega_{RF})t], \quad (2)$$

where A_{-1} and $A_1$are the amplitudes of the two input tones, respectively. ω_0 and ω_{RF} are the angular frequencies of the optical carrier and the input RF signal, respectively. By controlling ω_0, the right tone in wavelength is set at a resonance of the MRR. This tone is coupled to the drop port of the MRR, and the left tone is fed into the interleaver. Then, the two tones are combined by an MMI. The output of the IBPS can be written as:

$$E_{out} = \alpha_{-1}A_{-1}\exp[j(\omega_0 - \omega_{RF})t]\cdot\exp(j\theta_{-1}) + \alpha_1 A_1\exp[j(\omega_0 + \omega_{RF})t]\cdot\exp(j\theta_1), \quad (3)$$

where $\alpha_{\pm 1}$and $\theta_{\pm 1}$ are the amplitude gain and the optical phase shift, respectively. The signal is detected by a photo-detector (PD), and the output current is:

$$i_{AC}(t) \propto 2R\alpha_{-1}A_{-1}\alpha_1 A_1\cos[2\omega_{RF}t + (\theta_{-1} - \theta_1)], \quad (4)$$

where R is the amplitude response of the PD. The phase of the generated RF signal is θ_{-1} - θ_1. Since $\theta_{-1}$is fixed, the phase shift is determined by θ_1. As illustrated in Fig. 3, the change of θ_1 is realized by tuning the central wavelength of the interleaver. Here, we use a diameter of 86.7 μm

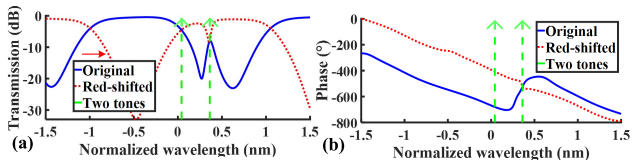

Fig. 3. Simulated wavelength tuning of (a) the transmission spectrum and (b) the phase response of the IBPS. Green dotted lines: the two tones of an OCS signal.

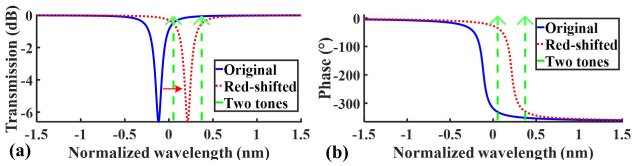

Fig. 4. Simulated wavelength tuning process with (a) the transmission spectrum and (b) the phase response of the MRR. Green dotted lines: the two tones of an OCS signal.

for the add-drop MRR to achieve the same FSR as that of the interleaver. The transmission coefficients of the thru port and the drop port of the MRR are 0.990 and 0.937, respectively. The flat-top passband transmission and the linear phase response of the interleaver enable a low power variation and a linear phase shift of the output RF signal.

The performance of the proposed IBPS is evaluated here with a figure of merit (FoM) in terms of RF phase-shift range, RF power variation and RF phase-shift linearity, and compared with the widely exploited MRR-based phase shifter. Most prior arts focused on the RF power variation and the RF phase-shift range. Some of them addressed the phase-shift linearity issue but there was no quantitative analysis [6], [7]. In our work, the RF phase-shift linearity is taken into account. Here we define the FoM with the performance indicators of interest, as expressed below:

$$\text{FoM} = \frac{\text{RF phase-shift range}(^\circ)}{\text{RF power variation (dB)} \times \text{Linearity}}. \quad (5)$$

In the quantification of the linearity, the phase deviation between the phase shifts and their linear fitting, and the RF phase-shift range should be considered. Thus we define the RF phase-shift linearity as:

$$\text{Linearity} = \frac{\text{maximum phase deviation } (^\circ)}{\text{RF phase-shift range } (^\circ)}. \quad (6)$$

In the simulation for the MRR-based phase shifter [12], the amplitude transmission coefficient of the coupling region is $t = 0.933$ and the radius of the ring is 20 μm. The loss factor α and the group index are the same as that in the simulation of the IBPS. As depicted in Fig. 4, the MRR-based phase shifter is simulated at an RF frequency of 40 GHz. A maximum FoM of 271 °/dB is achieved with an RF power variation of 6.21 dB and an RF phase shift of 274°, which are shown in Figs. 5(a) and (b), respectively.

For comparisons, the performance of the IBPS is also simulated with a 274° RF phase shift, which is presented in Figs. 5(c) and (d). In the case of the same RF phase shift, the IBPS exhibits a higher FoM of 2511 °/dB, a lower RF power variation of 3.41 dB and a better linearity of 0.032 compared to the MRR-based phase shifter. For the IBPS, different RF phase-shift ranges lead to different RF power variations.

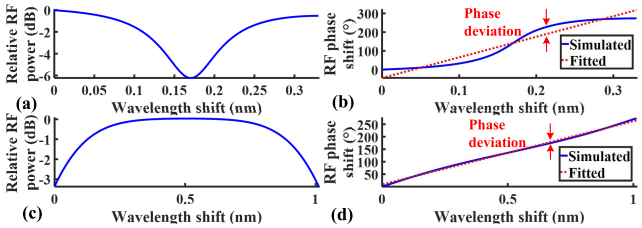

Fig. 5. (a) Relative RF power versus wavelength shift for the MRR-based phase shifter. (b) RF phase shift versus wavelength shift for the MRR-based phase shifter (blue-solid line) and its linear fitting (red-dotted line). (c) Relative RF power versus wavelength shift for the IBPS. (d) RF phase shift versus wavelength shift for the IBPS (blue-solid line) and its linear fitting (red-dotted line).

TABLE I
PERFORMANCE COMPARISON OF MICROWAVE PHOTONIC PHASE SHIFTERS

Structure	RF phase-shift range (°)	RF power variation (dB)	Linearity	FoM (°/dB)
MRR-based phase shifter	274	6.21	0.163	271
IBPS	274	3.41	0.032	2511
IBPS	190	1.01	0.023	8179
IBPS	360	8.74	0.027	1526

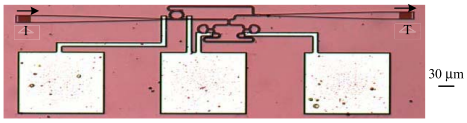

Fig. 6. The microscopic picture of the IBPS.

A tradeoff between the RF power variation and the RF phase-shift range should be considered. TABLE I summarizes the results.

III. FABRICATION, EXPERIMENTAL SETUP AND RESULTS

A. Fabrication

The device was fabricated on a SOI wafer with a 220-nm-thick silicon layer and a 3-μm-thick buried silicon dioxide layer. The silicon waveguide was etched by an inductively coupled plasma (ICP) etching process. Then, a 1-μm-thick silica layer was deposited on the top of the device as upper cladding by plasma enhanced chemical vapor deposition (PECVD). Fig. 6 shows the microscopic picture of the tunable IBPS. Two microheaters and three pads were formed by 100-nm-thick Ti and 1-μm-thick Al, respectively. The cross sections of the silicon waveguides are 450 nm $\times$ 220 nm. The diameter of the ring is 20 μm. The coupling gap (ring-to-waveguide gap) of the through port and the drop port are 200 nm and 260 nm, respectively. The coupling lengths of directional couplers for t_1 and t_2 are 3.1 μm and 1.4 μm, respectively, and both the coupling gaps are 200 nm. Grating couplers are employed for vertical coupling between the silicon chip and the single mode fibers.

B. Experimental Setup

Fig. 7 illustrates the experimental setup for system demonstration of the tunable IBPS. An optical carrier is output by a tunable laser source (Keysight 81960A), which is modulated by a 20-GHz RF signal generated from a microwave signal generator (APSIN20G) via a Mach-Zehnder modulator (MZM). Then the generated OCS signal is amplified by an erbium-doped fiber amplifier (EDFA). Two polarization controllers (PCs) are used to ensure that the polarization states of the optical waves are aligned to the MZM and the device. At the output port of the silicon chip, a 1:9 power splitter is used to split the output power into two parts. One part is detected by an optical spectrum analyzer (APEX AP2040C), and the other is amplified by an EDFA followed a tunable bandpass filter (BPF). The BPF is used to suppress the amplified spontaneous emission (ASE) noise. Then the filtered signal is detected by a PD. After the optical-to-electrical (O/E) conversion, a desired microwave signal is generated. An oscilloscope (Keysight DCA-X 86100D) is used to record the phase shift and the RF power of the received signal.

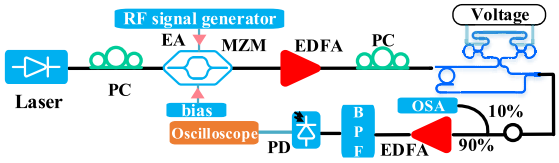

Fig. 7. Experimental setup for the measurement of the IBPS. EA: electrical amplifier. OSA: optical spectrum analyzer.

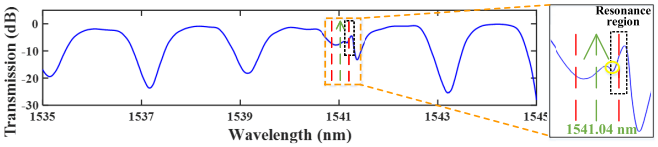

Fig. 8. Measured transmission spectrum of the device in the spectral range from 1535 nm to 1545 nm.

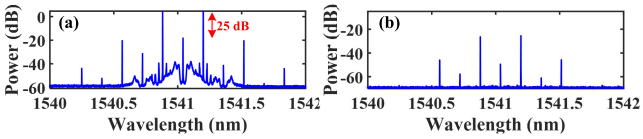

Fig. 9. Spectra of the OCS signal at the input (a) and output (b) of the device, respectively.

C. Experimental Results

The normalized measured transmission spectrum of the IBPS in the spectral range from 1535 nm to 1545 nm is shown in Fig. 8, where the resonance region of the add-drop MRR can be observed. The valley in the yellow circle of the zoom-in view can be attributed to the fabrication errors. To ensure a large phase shift in the passband, the resonance of the add-drop MRR is tuned to the stopband of the interleaver by using a thermo-optic heater. In this device, one of the resonance wavelengths is ~1541.20 nm. Thus, the wavelength of the input laser source is set at 1541.04 nm. The optical carrier is suppressed by biasing the MZM at the transmission null with a 25-dB suppression ratio, which is shown in Fig. 9(a). The suppression is sufficient to avoid the harmonic distortion. The spectrum of the OCS signal at the output port of the device is provided in Fig. 9(b). A loss of ~20 dB comes from the insertion loss of the fabricated device and the fiber-chip coupling losses. In the device, the losses of the drop port of

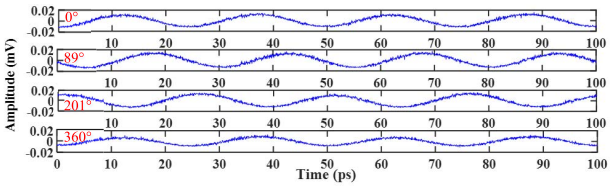

Fig. 10. Waveforms of the 40-GHz RF signal with different phase shifts.

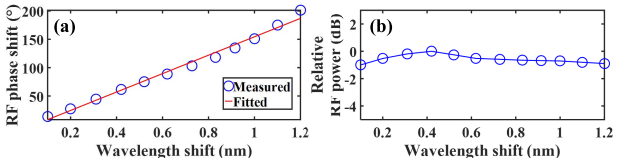

Fig. 11. Measured linear phase shift (a) and relative RF power (b) versus the wavelength shift.

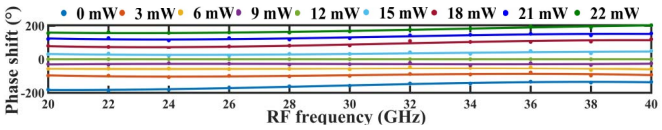

Fig. 12. Measured phase shifts for different heating powers over a frequency range from 20 GHz to 40 GHz.

the MRR, the interfering loop, and the MMI are ∼2.0 dB, ∼1.0 dB and ∼3.0 dB, respectively.

Fig. 10 depicts the waveforms of the generated RF signals with different phase shifts. When the applied heating power increases from 0 mW to 23.07 mW, a full 360° phase shift with a 3.9-dB RF power variation is achieved. The measured wavelength-tuning efficiency is ∼0.08 nm/mW. The RF gain was measured to be approximately −12.05 dB. In [13], a high-Q MRR was used to achieve a 336° phase shift with a 11-dB RF-signal power variation and a 1.6-mW power consumption. Inthe case of the same phase shift, the IBPS can achieve a relatively lower RF-signal power variation and a better linearity. The linear phase shift and the RF power variation as a function of the wavelength shift are provided in Fig. 11. The linearity of the measured phase shifts can be calculated by (6). As a result, a linear phase shift of 188° is achieved with a linearity of 0.08 and a <1-dB RF power variation.

The IBPS works with different RF frequencies. Fig. 12 shows the tunable RF phase shift range up to 320° over an RF bandwidth from 20 to 40 GHz. The microwave signal at a 12-mW heating power is used as a reference. For the top and bottom curves in Fig. 12, the left tone of the OCS signal is close to the stopband of the interleaver, which is the main cause of the phase distortions. In practical applications, one can use the central part of the passband to ensure a good linearity. Since the add-drop MRR filter with a bandwidth of ∼ 40 GHz is used to separate the two tones of an OCS signal, the minimal RF frequency is limited to 20 GHz. The power variation and the linearity of the device relate to the wavelength dependences of the directional couplers, which set fundamental limits on the performance of the device in terms of the power variation and the linearity.

It should be noted that any interleavers with flat-top passbands and linear phase responses can be used to realize RF phase shifters. The maximum phase shift, the RF power variation, and the phase-shift linearity highly depend on the performance of the interleaver employed. The upper bound of the RF frequency is limited by the passband width of the interleaver. Note that in our device only one tone needs to be tuned in phase while the other one remains fixed, which is different from a conventional true time delay line. The optical single sideband modulation with full carrier (OSSB+C) can also be used with our device to generate an optical delay on the modulated RF signal, which is similar to the scheme employed in [14].

IV. Conclusion

In this letter, an RF phase shifter based on an interleaver was proposed and experimentally demonstrated. The IBPS exhibits an FoM improvement from 271 °/dB to 2511 °/dB relative to the MRR-based phase shifter, based on numerical calculations. The experimental results showed a 360° phase shift with an RF power variation of 3.9 dB, or a linear 188° phase shift with an RF power variation of less than 1 dB at the 40-GHz RF frequency. The linearity of the IBPS was 0.08 with the phase-shift tuning range of 188°. A tunable phase shift of 320° over an RF frequency range from 20 to 40 GHz was also experimentally demonstrated.

Acknowledgment

The authors wish to thank the Center for Advanced Electronic Materials and Devices of Shanghai Jiao Tong University for the support of device fabrication.

References

[1] J. Capmany and D. Novak, "Microwave photonics combines two worlds," *Nature Photon.*, vol. 1, no. 6, pp. 319–330, Apr. 2007.
[2] R. A. Minasian, E. H. W. Chan, and X. Yi, "Microwave photonic signal processing," *Opt. Express*, vol. 21, no. 19, pp. 22918–22936, Sep. 2013.
[3] J. Capmany, J. Mora, I. Gasulla, J. Sancho, J. Lloret, and S. Sales, "Microwave photonic signal processing," *J. Lightw. Technol.*, vol. 31, no. 4, pp. 571–586, Feb. 15, 2013.
[4] Z. Cao *et al.*, "Advanced integration techniques on broadband millimeter-wave beam steering for 5G wireless networks and beyond," *IEEE J. Quantum Electron.*, vol. 52, no. 1, Jan. 2016, Art. no. 0600620.
[5] L. Gao and K. H. Wagner, "Wavelength-compensated photonic multibeam-forming system for two-dimensional wideband radio-frequency phased-array antennas," *Appl. Opt.*, vol. 48, no. 22, pp. E1–E12, Aug. 2009.
[6] M. Pu *et al.*, "Widely tunable microwave phase shifter based on silicon-on-insulator dual-microring resonator," *Opt. Express*, vol. 18, no. 6, pp. 6172–6182, Mar. 2010.
[7] J. Capmany, D. Domenech, and P. Muñoz, "Silicon graphene waveguide tunable broadband microwave photonics phase shifter," *Opt. Express*, vol. 22, no. 7, pp. 8094–8100, Apr. 2014.
[8] S. Cao *et al.*, "Interleaver technology: Comparisons and applications requirements," *J. Lightw. Technol.*, vol. 22, no. 1, pp. 281–289, Jan. 2004.
[9] C. K. Madsen and J. H. Zhao, *Optical Filter Design and Analysis: A Signal Processing Approach*. New York, NY, USA: Wiley, 1999, pp. 114–119.
[10] Q. J. Wang, Y. Zhang, and Y. C. Soh, "Design of linear-phase two-port optical interleavers using lattice architectures," *Opt. Lett.*, vol. 31, no. 16, pp. 2411–2413, Aug. 2006.
[11] X. Jiang *et al.*, "Design and experimental demonstration of a compact silicon photonic interleaver based on an interfering loop with wide spectral range," *J. Lightw. Technol.*, vol. 35, no. 17, pp. 3765–3771, Sep. 1, 2017.
[12] Q. Chang, Q. Li, Z. Zhang, M. Qiu, T. Ye, and Y. Su, "A tunable broadband photonic RF phase shifter based on a silicon microring resonator," *IEEE Photon. Technol. Lett.*, vol. 21, no. 1, pp. 60–62, Jan. 1, 2009.
[13] M. Pu *et al.*, "Tunable microwave phase shifter based on silicon-on-insulator microring resonator," *IEEE Photon. Technol. Lett.*, vol. 22, no. 12, pp. 869–871, Jun. 15, 2010.
[14] M. Burla *et al.*, "On-chip CMOS compatible reconfigurable optical delay line with separate carrier tuning for microwave photonic signal processing," *Opt. Express*, vol. 19, no. 22, pp. 21475–21484, Oct. 2011.